Physical Biology

PAPER

# Morphology and dynamics of tumor cell colonies propagating in epidermal growth factor supplemented media

RECEIVED
2 January 2018

REVISED
26 March 2018

ACCEPTED FOR PUBLICATION
6 April 2018

PUBLISHED
30 April 2018

N E Muzzio[1], M Carballido[2], M A Pasquale[1,4], P H González[3], O Azzaroni[1] and A J Arvia[1]

[1] Instituto de Investigaciones Fisicoquímicas Teóricas y Aplicadas (INIFTA), Universidad Nacional de La Plata (UNLP), CONICET, Sucursal 4, Casilla de Correo 16, 1900, La Plata, Argentina
[2] Facultad de Ciencias Exactas, UNLP, Calle 47 y 116, 1900, La Plata, Bs. As., Argentina
[3] Cátedra de Patología, Facultad de Ciencias Médicas, UNLP, CICBA, Calle 60 y 120, 1900, La Plata, Bs. As., Argentina
[4] Author to whom any correspondence should be addressed.

**E-mail:** miguelp@inifta.unlp.edu.ar

**Keywords:** epidermal growth factor, HeLa cell, colony kinetics, dynamic scaling

Supplementary material for this article is available online

## Abstract

The epidermal growth factor (EGF) plays a key role in physiological and pathological processes. This work reports on the influence of EGF concentration ($c_{EGF}$) on the modulation of individual cell phenotype and cell colony kinetics with the aim of perturbing the colony front roughness fluctuations. For this purpose, HeLa cell colonies that remain confluent along the whole expansion process with initial quasi-radial geometry and different initial cell populations, as well as colonies with initial quasi-linear geometry and large cell population, are employed. Cell size and morphology as well as its adhesive characteristics depend on $c_{EGF}$. Quasi-radial colonies (QRC) expansion kinetics in EGF-containing medium exhibits a complex behavior. Namely, at the first stages of growth, the average QRC radius evolution can be described by a $t^{1/2}$ diffusion term coupled with exponential growth kinetics up to a critical time, and afterwards a growth regime approaching constant velocity. The extension of each regime depends on $c_{EGF}$ and colony history. In the presence of EGF, the initial expansion of quasi-linear colonies (QLCs) also exhibits morphological changes at both the cell and the colony levels. In these cases, the cell density at the colony border region becomes smaller than in the absence of EGF and consequently, the extension of the effective rim where cell duplication and motility contribute to the colony expansion increases. QLC front displacement velocity increases with $c_{EGF}$ up to a maximum value in the 2–10 ng ml$^{-1}$ range. Individual cell velocity is increased by EGF, and an enhancement in both the persistence and the ballistic characteristics of cell trajectories can be distinguished. For an intermediate $c_{EGF,}$ collective cell displacements contribute to the roughening of the colony contours. This global dynamics becomes compatible with the standard Kardar–Parisi–Zhang growth model, although a faster colony roughness saturation in EGF-containing medium than in the control medium is observed.

## 1. Introduction

The stimulation of cell growth and motility plays a key role in many physiological and pathological processes such as morphogenesis, wound healing and tumor propagation, the coordinated displacement of cells being of relevance [1–4]. The epidermal growth factor (EGF) stimulates a large number of cell phenotypes involved in those biological processes [5–8]. EGF binds a plasma membrane receptor tyrosine kinase [9] and enhances cell proliferation and migration. However, the effect of EGF depends on the cell type, either normal or neoplastic, triggering important mechanisms differently according to the cell type [10]. It has also been reported from scratch assays of intestinal epithelial cell data [11] that EGF-induced cell motility patterns render a repopulated zone with a larger number of voids in comparison with control experiments involving other stimulating species. In fact, a milieu of growth factors is secreted immediately after wounding, and the relation of each one to cell motility behavior is of relevance for interpreting the underlying mechanism of the repopulation process [12].

On the other hand, the EGF-induced cell scattering *in vitro* model for studying epithelial-mesenchymal transition (EMT) recapitulates many events that occur during EMT, including the dissociation of multicellular structure and increased cell motility [13]. More recently, it has been reported that individual cell motility is affected by either soluble [14, 15] or immobilized EGF [16, 17], increasing the collective monolayer displacement, although in the case of immobilized EGF, there is a significant increase in the cell displacement persistence. Cell movements are often guided by chemical cues, and the chemoattractant molecules bind to surface receptors on the membrane and activate intracellular signals. In general, cells move in interacting groups rather than in an isolated manner [18, 19]. Although the mechanism of individual cell motion induced by chemoattractants has been rather extensively studied, the displacement characteristics of cell groups determining their directionality is much less understood [20]. It has been reported that cell–cell communication enhances the sensitivity of cell ensemble to chemoattractant gradients [21].

Recently, it has been reported that the collective displacement undergoes by intermittent bursts of certain extensions of the cell monolayer, similar to those observed in the flow of liquids in porous media. This behavior is independent of the type of cell and the nature of the substrate [22]. Other universal behaviors, found either in inanimate or living systems, have also been reported [23–25]. Constituents of living systems interact in a cooperative manner and determine the global system behavior. Then, for instance, the properties of the resulting interface can be described by its fractality by applying different statistical techniques such as the dynamic scaling analysis to access the spatial and scale dependence of colony interface fluctuations. In this approach, the two-dimensional (2D) cell colony front dynamics can be interpreted based upon a set of dynamic scaling exponents ($\alpha, \beta, z$, the roughness, the growth and the dynamic exponents, respectively) derived from the dynamic scaling analysis of colony front profiles, and by comparing these results to those expected from different statistical growth models [26, 27]. Experimental data from non-Euclidean 2D spreading biological interfaces were interpreted, at least within certain ranges of colony front length and age, in terms of the standard Kardar, Parisi and Zhang (KPZ) continuous equation [28–30]. The evolution of other systems in nature has been recently analyzed in terms of the KPZ model, such as wall roughness of two-dimensional Pt/Co/Pt thin films [31], the growth of semiconductor thin films [32], among others. A characteristic feature of the standard KPZ equation is the nonlinear term that in the case of cell colonies can be related to the anisotropic cell displacements towards free space at the colony border [26, 33].

A large number of studies aiming to elucidate several biochemical mechanisms in which either EGF or its receptors play a key role have been reported [34]. In contrast, papers dealing with the effect of EGF on the global cell colony dynamics [35] of different initial geometry and cell population are rather scarce. The cell colony front velocity data, measured from the average colony radius ($\langle R \rangle$) of initial quasi-radial colonies (QRCs), or the linear average displacement distances from a reference position, in the case of quasi-linear colonies (QLCs), allow us to distinguish the effect of some cooperative behavior modulated by EGF concentration ($c_{EGF}$) on the global dynamics. Several works have demonstrated the increase in cell motility for a certain range of $c_{EGF}$ [36, 37] and the dispersion effect on cell colonies [13]. In the same vein, the hepatocyte growth factor (HGF) has been employed to perturb the colony border expansion pattern by inducing cell dispersion [38]. Considering these facts, it is interesting to hypothesize that EGF would change some characteristics of the roughness fluctuation process due to its mitogenic and motogenic effect described in the frame of the KPZ equation and integrating phenomena at the cellular and colony scale.

In the present work, colonies that remain confluent during the follow-up are susceptible of being characterized by their displacement distance and their roughness evolution. Results show that within certain range of $c_{EGF}$, the colony front dynamics depends on both the initial cell population and the colony cell density. Accordingly, the presence of EGF contributes to modifying the local cell density heterogeneity by local changes in the size and shape of the cells, affecting cell motility characteristics. The latter effect involves a first cell adhesion step followed by its expansion and propagation, i.e. all these processes depend on the cytoskeleton reorganization. The presence of EGF modifies the amount and size of focal contacts. Furthermore, in the presence of EGF within a certain concentration range, cell displacements become more persistent and ballistic and with a greater contribution of lateral components than in the plain medium, influencing the global dynamics of large population colonies characterized by the front roughness evolution. Thus, dynamic data from colonies growing in EGF-containing medium are consistent with the predictions of the standard Kardar–Parisi–Zhang equation, although the roughness saturation is approached earlier than for cell colonies in the control medium.

## 2. Experimental

### 2.1. Colony preparation procedures

HeLa cells, passage 44–60, were employed. Cell colonies were cultured in polystyrene Petri dishes 3.6 cm in diameter (Greiner Bio One), employing Roswell Park Memorial Institute (RPMI) medium supplemented with 10 % fetal bovine serum (FBS), 2 g $l^{-1}$ bicarbonate, and 100 $\mu$M $ml^{-1}$ streptomycin. Epidermal growth factor in the 0–50 ng $ml^{-1}$ concentration range was added to the culture medium. The cultures were incubated at 37 °C in a sterilized atmosphere with 5%

carbon dioxide and 97% humidity. As required, half of the medium was changed every 2 d to maintain its composition practically constant. Cell viability was achieved by Trypan blue vital staining. The culture medium, antibiotic and EGF were acquired from Life Technologies.

Each QRC was grown by seeding 2 ml of supplemented medium containing 1000–2000 cells into Petri dishes, where they adhere to the dish bottom. After growing for 4–5 d, the culture consisted of colonies with a different number of cells ($N_0$) at the time $t_0$ at which colony growth data collection started.

QLCs were prepared as described elsewhere [30] utilizing a sterilized Teflon® tape 2.2 cm wide and 100 $\mu$m thick to cover the central region of a Petri dish bottom. Subsequently, 2 ml of a suspension of 20 000 cells ml$^{-1}$ in supplemented medium was seeded. Cell duplication produced a number of colonies spreading on the remaining Petri dish bottom free surface. Then, about 2 d later, when a confluent cell monolayer was formed, the Teflon tape was removed. In these runs, in contrast to QRC colonies, to avoid the influence of cell confinement, spreading data were collected about 12 h after removing the Teflon tape.

### 2.2. Colony growth pattern microimaging

Colony growth patterns were imaged using a Nikon DS-Fi digital camera coupled to a Nikon TS100 phase-contrast inverted microscope with a CFI flat field ADL 10× objective. The image resolution was 1 $\mu$m = 2.1 pixel. The colony growth time ($t$) was counted from $t_0$, the time from which data were collected, except for those experiments in which another reference time was selected, as is indicated further on.

*In situ* cell colony digital images were obtained for 2–3 d by a time-lapse system at intervals in the range $5 \leqslant \Delta t' \leqslant 45$ min. For this purpose, QLCs were placed inside an isolated chamber fixed to the microscope platform to maintain the cultures at 37 °C and 97% humidity. For preserving the pH, before placing each Petri dish in the chamber, the culture medium was changed to RPMI $CO_2$-Independent Medium (Gibco, Invitrogen Corp.). Occasionally, the culture medium was replaced by fresh RPMI bicarbonate supplemented medium under a 5% $CO_2$-air atmosphere. Both media contained L-glutamine and streptomycin.

### 2.3. Cell immunostaining

Fluorescent staining of vinculin, actin and cell nucleus was carried out to study cell adhesion. The staining was done following the protocol described in the Actin Cytoskeleton and Focal Adhesion Staining Kit user manual. Cultured cells were washed with PBS containing 0.05% Tween-20 and fixed with 4% paraformaldehyde. Then, glass cover slips were washed, and cells were permeabilized with 0.1% Triton X-100 in PBS for 5 min. After washing, a blocking solution, 1% BSA in PBS, was applied for 30 min. Then, the antivinculin antibody diluted in the blocking solution was added and incubated for 1 h, followed by washing. The anti-mouse IgG-FITC conjugated antibody diluted in PBS was added to the samples and incubated for 1 h. TRITC-conjugated phalloidin was incubated simultaneously with the second antibody for double labelling. After washing, nucleus counterstaining was performed by incubating cells with DAPI for 5 min. These samples were washed and mounted on a slide by using antifade mounting solution. Stained cells were observed by an Epi-fluorescence IX 50 Olympus microscope. The number and area of focal contacts were evaluated employing ImageJ software and following the procedure proposed in [39].

### 2.4. Colony data processing

Colony fronts were manually traced using a Wacom graphic table; the trace error from zoomed images of colony growth patterns resulted in the order of 1 pixel. For data processing, an in-lab developed program was utilized. For QLC at time $t$, the instantaneous vertical advancing distance, the height of the $i$th point at the colony front ($h_i(t)$, $i = 1, 2, \ldots n$), and the mean colony distance $\langle h \rangle = \sum_i h_i(t)/n$ were evaluated. Similarly, for QRC the colony center of mass (CM), the instantaneous distance ($R_i(t)$) from CM to the $i$th point at the front, and the mean colony radius $\langle R \rangle = \sum_i R_i(t)/n$ were determined.

For QLC with front of size $L$, the instantaneous global roughness of the expanding front was determined as the standard deviation of the height fluctuations

$$w(L,t) = \left\{ \frac{1}{N} \sum [h_i - \langle h \rangle]^2 \right\}^{1/2}. \qquad (1)$$

In this equation, $h_i$ is the maximum instantaneous height at each $i$ point of the colony border. The local roughness, $w(l,t)$, of each colony front was determined in the range $100 \leqslant l \leqslant L$ $\mu$m.

### 2.5. Individual cell trajectories

Trajectories of selected cells were measured from the instantaneous 2D coordinates ($\mathbf{P}_j = \mathbf{p}(t_i) = x_j(t_i)$, $y_j(t_i)$, $t_i = 1, 2, \ldots n$) by manually tracking time-lapse movie frames employing Image-Pro Plus 6.0 software, Media Cybernetics Inc.

Coordinate evaluations were referred to either the cell nucleus or the centroid position of each cell contour drawn. From an average of 10 trajectories followed for about 24 h, the difference between both procedures was about 10%. From coordinate data, the mean cell velocity $\langle V_i \rangle$ was evaluated from the equation

$$\langle V_i \rangle = \frac{\mathbf{p}_j(t_{i+1}) - \mathbf{p}_j(t_i)}{\Delta t'}. \qquad (2)$$

Celerity, velocity components parallel ($V_{\mathrm{par}}$) and perpendicular ($V_{\mathrm{per}}$) to the colony front were evaluated within the interval $15 \leqslant \Delta t' \leqslant 45$ min. Considering the small error in the determination of

each cell nucleus location, the same average velocity was obtained irrespective of the values of $\Delta t'$.

The mean square displacement was evaluated from the following equation

$$\text{msd} = \left\langle \left( (x_i(t_0 + \Delta t) - x_i(t_0))^2 \right) + \left( (y_i(t_0 + \Delta t) - y_i(t_0))^2 \right) \right\rangle \quad (3)$$

where $t_0$ is the starting time of the recording interval ($\Delta t$). Average data from all values of $t_0$ and all cell trajectories were derived following [40].

The msd dependence on $\Delta t$ approached the power law

$$\langle \text{msd}(\Delta t) \rangle \propto (\Delta t)^b \quad (4)$$

the constant $b$ being 1 for a cell with random walk displacement, and 2 for a cell with ballistic displacement [41].

The persistence was calculated as the time needed for the cell to change its displacement direction by 45°.

Cell motility was also studied by particle image velocimetry [42] using PIVlab 1.35 software [43] for MATLAB (The MathWorks, Natick, MA). Image sequences recorded for 500 min with $\Delta t'$ in the 15–45 min range were filtered and analyzed with an interrogation window of 82 × 82 pixels with 50% overlap.

## 3. Results

### 3.1. Quasi-radial colonies

#### 3.1.1. Morphology

QRCs were grown in a culture medium supplemented with $c_{EGF} = 0, 0.08, 0.4, 2$ and 10 ng ml$^{-1}$, and followed by optical microscopy. The follow-up covered the first stages of the colony growth up to 10 000 min and only colonies that remain confluent were considered (figure 1). QRCs with $N_0 < 100$ cells, cell density $< 0.0007$ cells $\mu$m$^{-2}$, in culture media with $c_{EGF} > 0.4$ ng ml$^{-1}$ rendered disaggregated colonies that were not susceptible to be quantitatively followed up by their average radius (see supplementary data, SI (stacks.iop.org/PhysBio/15/046001/mmedia)).

In the absence of EGF (figures 1 and S1), at the first stages of growth the average cell size remained almost constant, but the local cell density increased at the colony bulk and diminished at the colony border region. Finally, at longer stages of growth, the incipient appearance of a 3D phase of cells, cell aggregates above the monolayer, at inner colony regions was observed. In previous works we described the cell 3D phase formation more completely, and showed stained colonies to allow a clearer visualization of cell aggregates [29, 33].

On the other hand, colonies growing in the $c_{EGF} = 0.4$ ng ml$^{-1}$ medium for $t$ up to about 2000 min (figure 1(b)) exhibited a cell density decrease along the whole colony, but later, the cell density increased and tended to remain rather uniform over the entire colony.

For $c_{EGF} = 10$ ng ml$^{-1}$, a typical cell colony with $N_0 \approx 1300$ cells and an initial cell density close to 0.002 72 cells $\mu$m$^{-2}$ (figure 1(c)) exhibited a first slight colony density decrease at border regions, then a large cell density increase at inner colony regions, and at longer time the formation of a homogeneously distributed 3D cell phase made of quasi-spherical cells of 10 $\mu$m diameter or thereabouts. It is worth noting that the cell morphology evolution and the dynamics of 3D phase formation differ considerably from that observed above either in the absence of EGF or at relatively low $c_{EGF}$. In the former, the 3D phase is made up of a large number of rounded disaggregated cells or small groups of them, whereas for the latter, the 3D phase consists of highly dense cell aggregates. As has been described previously [29], at inner regions of the colony with appropriate cell density, there would be a space restriction for either cells at the monolayer or new born cells to interact with the substrate, tending to locate on upper planes above the monolayer and forming rather compact aggregated or disaggregated cells for $c_{EGF} = 0$ or in the presence of EGF, respectively.

At $c_{EGF} = 2$ ng ml$^{-1}$, individual cell morphological characteristics (figure 2(a)) indicated that the cell spreading area was smaller than in the absence of EGF. Concomitantly, the cell–cell contact area diminished, and a large number of cells exhibited long filopodia connections. Furthermore, in these cases, cell immunostaining of vinculin protein provided information about both focal contacts between cells and the substrate. As $c_{EGF}$ increased, the number of focal contacts increased although their average size diminished (figure 2(b)); these features were similar for $c_{EGF} = 10$ ng ml$^{-1}$, tending to reach a saturation effect for higher $c_{EGF}$. The distribution of focal contacts also depended on $c_{EGF}$. For cells in the control medium, focal contact distribution was rather homogeneous in the cell cytoplasm surrounding the nucleus. In contrast, in the presence of EGF, a large number of cells exhibited an increased focal contact density asymmetrically distributed. This fact was accompanied by the cytoplasm asymmetric spreading, as was more clearly appreciated by actin staining (figure 2(a)).

#### 3.1.2. Kinetic data

HeLa QRCs with a value of $N_0$ yielding confluent colonies along the entire follow-up for all $c_{EGF}$ allowed us to compare the kinetic behavior of colonies in the control and EGF-containing media. In these cases, the initial colony radius ($R_0$) in the 200–600 $\mu$m range was measured. The evolution of $\langle R \rangle$ depicted as log $\langle R \rangle$ versus $t$ plots offers the possibility of a better distinction of changes in the kinetic behavior of the systems (figure 3).

Cell colonies in the control medium, $c_{EGF} = 0$ ng ml$^{-1}$, followed up for about 10 d, showed an average

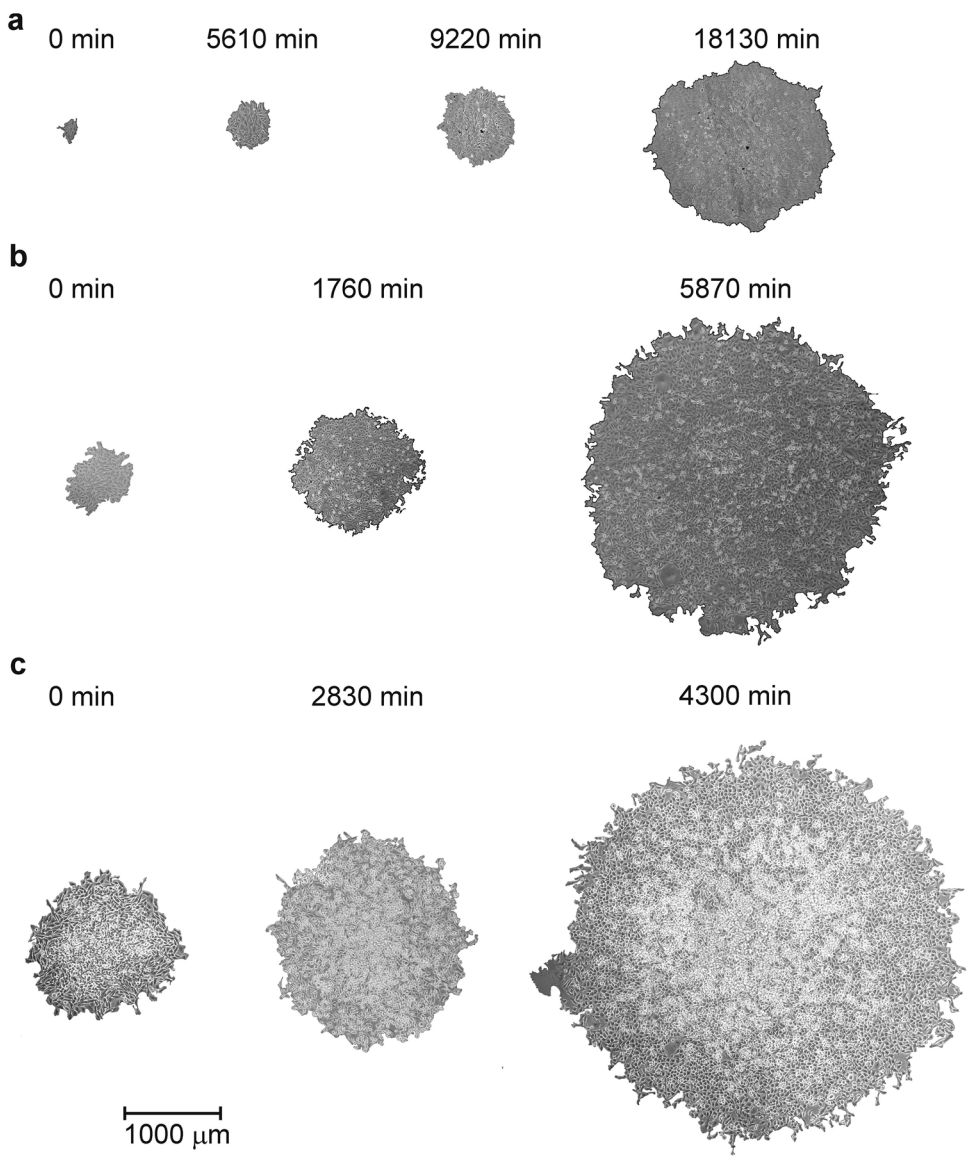


**Figure 1.** Evolution of cell colony growth pattern sequences in culture media supplemented with $c_{EGF}$: (a) 0; (b) 0.4; and (c) 10 ng ml$^{-1}$.

colony radius displacement $\langle R\rangle$ versus $t$ that follows an exponential law in the range from $t_0$ up to $t_c$, but for $t > t_c$ and $\langle R\rangle > \langle R_c\rangle$, a constant front displacement velocity ($V_F$) regime was attained, in agreement with the departure from the log $\langle R\rangle$ versus $t$ linear relationship (figure 3). From the exponential $V_F$ dependence, the average velocity constant $k = 4.2\ 10^{-4}$ min$^{-1}$ was obtained [33]. In the presence of EGF, the dependence of the colony radius on $t$ becomes more complicated than that observed for the control medium. In general, the colony front displacement velocity increases with $c_{EGF}$, but exhibits a relationship that depends also on the colony history. Values of $\langle R_0\rangle$, $N_0$ and the initial cell density are larger for colonies growing in EGF containing media in order to obtain confluent colonies over the entire growth time range.

As depicted in figure 3(b), $\langle R\rangle$ versus $t$ plots for the lowest $c_{EGF}$ showed only minor differences in comparison with the control medium. The colony growth kinetics exhibited the exponential regime followed by the constant velocity one, as referred to above. For relatively small $\langle R_0\rangle$ and initial densities, i.e. 0.0011 and 0.000 71 cell $\mu$m$^{-2}$, at the initial stages of growth $\langle R\rangle$ showed a supra-exponential dependence on $t$. Thus, $V_F$ increased faster than what should be expected from the exponential $\langle R\rangle$ versus $t$ relationship.

For colonies with comparable values of $N_0$ and cell density and with either $c_{EGF} = 0.4$ or 2 ng ml$^{-1}$ (figures 3(c) and (d)), the supra-exponential regime occurred for $0 < t < 4000$ min, with an average colony radius versus $t$ slope larger than that predicted by the exponential relationship. This trend also emerged for colonies growing in 10 ng ml$^{-1}$ (figure 3(d)). Accordingly, for $c_{EGF} = 10$ ng ml$^{-1}$ and colonies starting from $R_0 \sim 500$ $\mu$m ($N_0 \approx 1400$ cells), the supra-exponential kinetic regime followed by the exponential one remains up to about 9000 min. Later, the constant velocity regime is approached. For $\langle R_0\rangle < 500$ $\mu$m

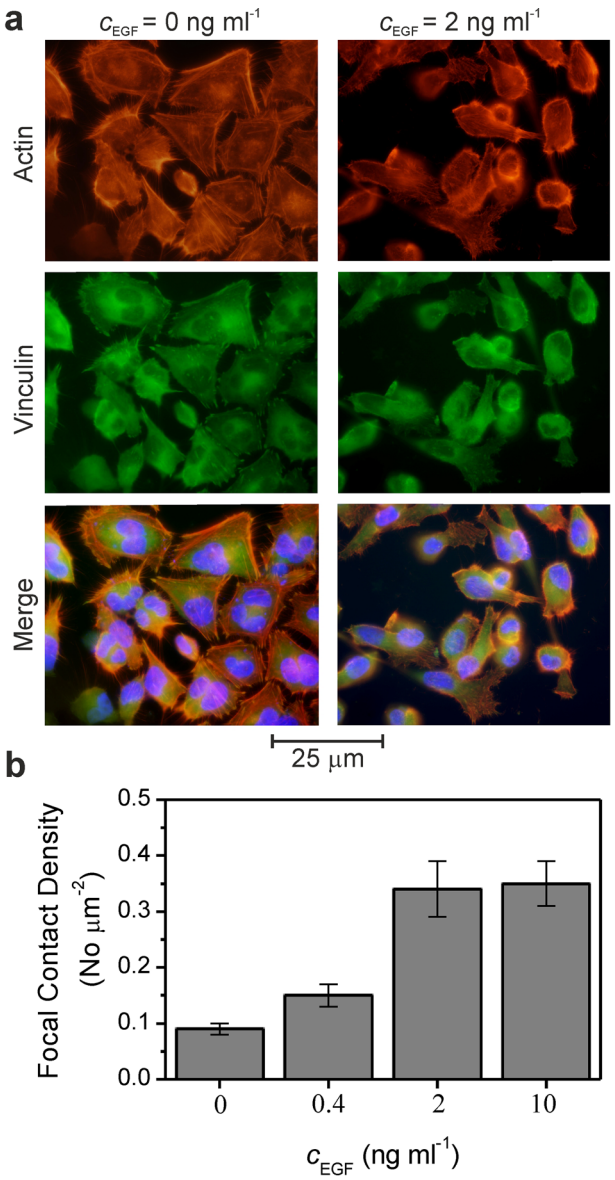


**Figure 2.** (a) Actin and vinculin immunostaining and merge with DAPI nucleus staining for cells seeded from control culture medium and $c_{EGF} = 2\,\text{ng ml}^{-1}$. (b) Histogram of the number of focal contacts in cytoplasms per $\mu\text{m}^2$ for cells seeded from control medium $c_{EGF} = 0\,\text{ng ml}^{-1}$, $c_{EGF} = 0.4\,\text{ng ml}^{-1}$, $c_{EGF} = 2\,\text{ng ml}^{-1}$, and $c_{EGF} = 10\,\text{ng ml}^{-1}$.

and $c_{EGF} = 10\,\text{ng ml}^{-1}$, the constant velocity regime is absent, and the exponential colony growth extends over the full observation time.

The departure of log $\langle R \rangle$ versus $t$ from the exponential colony growth kinetics at the initial stages of growth in the presence of EGF can be correlated with the colony morphology, i.e., the local change in cell density. Figure 4 shows typical $\langle R \rangle$ versus $t$ plots and their cell colony growth pattern evolution. In the presence of EGF, either for $c_{EGF} = 0.4\,\text{ng ml}^{-1}$ or $c_{EGF} = 10\,\text{ng ml}^{-1}$, at the first stages of growth, the supra-exponential regime can be distinguished. This effect becomes clearer for runs with $c_{EGF} = 0.4\,\text{ng ml}^{-1}$ than for $c_{EGF} = 10\,\text{ng ml}^{-1}$. However, the larger $c_{EGF}$ the greater the colony radius required to attain the constant velocity regime. From the colony pattern evolution, the decrease in the cell density at the colony inner regions can be observed over the time range of supra-exponential growth. In the insets of cell colony images, an increase in cell size, cell–cell separation, the presence of small voids, and a more tapered cell shape can be observed. Later, the departure from the log $\langle R \rangle$ versus $t$ linear relationship is accompanied by a significant increase in the colony cell density. The cell colony remains confluent although cell–cell interactions are expected to change with time and at the different growth kinetic stages depending in part on the cell shape and cell–cell contact area.

Colony growth kinetic data, at the first stages of growth, fit a $Bt^{1/2} + A'\exp(Ct)$ equation (with $B$, $A'$ and $C$, constants that depend on the experimental conditions), and at longer time they fit an equation that describes the transition from the exponential to the constant velocity growth regime as has been proposed by Drasdo *et al* [44] (color traces in figure 4). The proposed equation for the initial stages of the

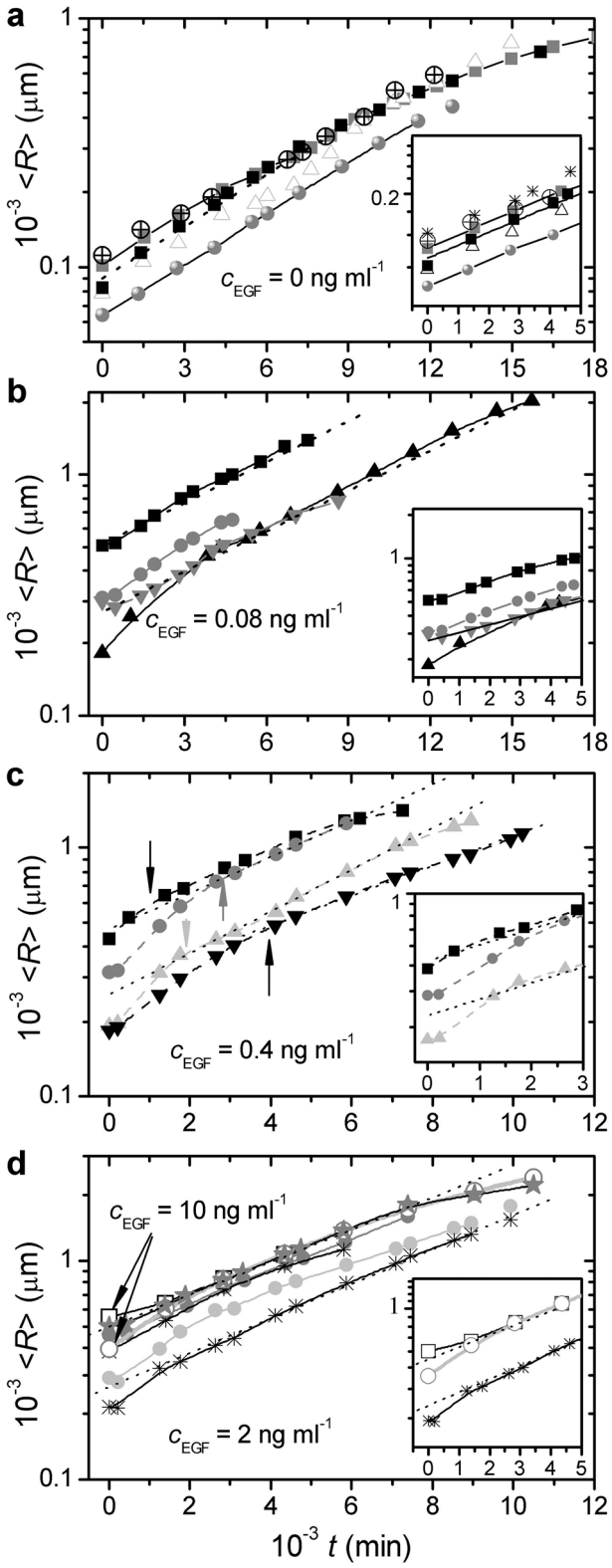


**Figure 3.** Semi-log $\langle R \rangle$ versus $t$ plots from HeLa QRCs grown in media with different $c_{EGF}$ as indicated in the figure. Lines to guide the eyes are depicted in dashed traces. Insets in the figure show the departure from the linear relationship at short $t$. Arrows in (c) indicate the transition time from the supra-exponential to the exponential growth regime.

colony growth contains two time-dependent terms, one related to cell motion and the other to cell proliferation. Diffusion is characterized by the $t^{1/2}$ dependence, and has been proposed for modeling cell colony growth at short times [28, 45]. This matter is further reconsidered in the discussion section.

Summing up, the complex kinetics of the cell colony growth depends on the value of $c_{EGF}$, the initial colony radius and cell density, as well as on the evolution of the cell density distribution in the colony. The cell colony growth is accompanied by the development of spatiotemporal heterogeneity cell distribu-

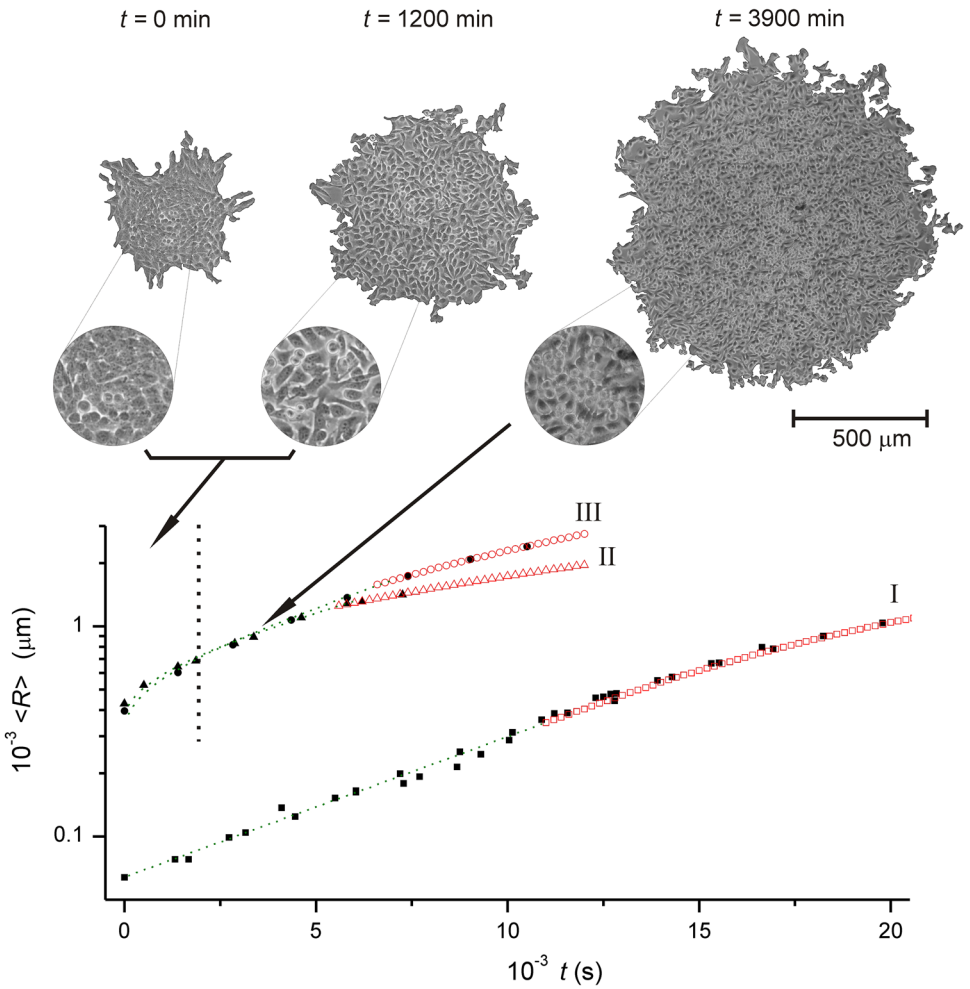


**Figure 4.** $\langle R\rangle$ versus $t$ plots for $c_{EGF} = 0$ (I), 0.4 (II), and 10 ng ml$^{-1}$ (III). In this case, each plot depicted in green and red discontinued traces corresponds to the adapted equations proposed by Drasdo *et al* [44] (details are included in the text). The cell colony pattern for $c_{EGF} = 0.4$ ng ml$^{-1}$ related to each distinctive growth kinetic regime is also included. Changes in cell morphology and density can be appreciated from the augmented insets.

tion at the colony. Table S1 of the supplementary data depicts $N_0$, $\langle R_0\rangle$, the initial density and the prevailing growth kinetic regime at different $c_{EGF}$. For colonies with both high $N_0$ and high initial cell colony density, the transition from exponential to constant velocity growth becomes more favorable. The time range of the exponential colony growth increases with $c_{EGF}$. The presence of EGF modifies the overall kinetics by changing the cell shape and size, cell–cell separation and increasing both the cell motility and duplication rate. Concomitantly with these effects, changes in both cell–cell and cell-substrate interactions are observed. These biochemical features depend on the initial cell colony population and density, and at least in part, they appear to be also reflected in the QRC growth kinetics, as at earlier stages of growth these colonies eventually exhibited a supra-exponential growth regime together with an increase in the cell colony front velocity and changes in $t_c$ and $N_c$ in the presence of EGF.

For runs made with 0.4 and 2 ng ml$^{-1}$, the cell density profile evolution (figure 5) depends on $N_0$ and the initial cell density, which is consistent with the preceding kinetic description. Thus, at the first stages of growth, QRCs with a low $N_0$ and a high initial cell density showed a rather abrupt decrease in cell density followed by its steady increase for $t \approx 5000$ min, up to density values close to or larger than that observed at $t_0$. The above decrease in cell density profile is consistent with the departure from the $\langle R\rangle$ versus $t$ exponential relationship observed at the initial stages of growth. At the initial stages of growth, for QRCs growing in culture medium with $c_{EGF} = 0.4$ ng ml$^{-1}$, a large $N_0$ and a small initial cell density, no cell density decrease at the initial stages of growth could be clearly distinguished. Correspondingly, the $\langle R\rangle$ versus $t$ plot exhibited a constant colony front displacement velocity over the entire growth time range. For $c_{EGF} = 2$ ng ml$^{-1}$ the decrease in the initial cell density is reflected in the appearance of the supra-exponential growth regime; the greater the initial density the more distinguishable the supra-exponential regime (figure 5). $N$ versus $t$ plots are included in figure 5 for the same experiments described above, exhibiting only a quasi-exponential behavior without the supra-exponential regime observed from $\langle R\rangle$ versus $t$ data.

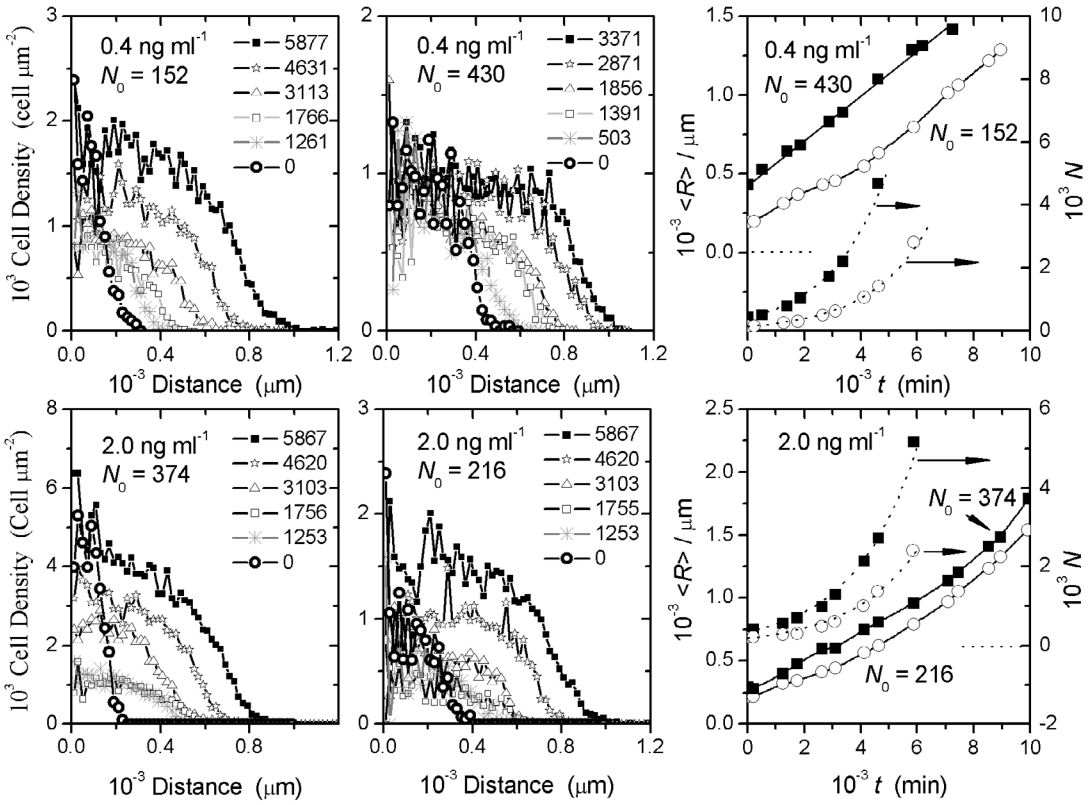


**Figure 5.** Density profiles and $\langle R\rangle$ versus $t$ plots from HeLa cell colonies with different initial cell populations and cell density growing in culture media with different $c_{EGF}$ as indicated. Those colonies exhibiting a decrease in the cell density at the first stages of growth either for $c_{EGF} = 0.4$ ng ml$^{-1}$ or $c_{EGF} = 2$ ng ml$^{-1}$ show a supra-exponential relationship in the $\langle R\rangle$ versus $t$ plots for $t$ up to 4000 min. $N$ versus $t$ data are also depicted for each experimental condition. The initial cell number for each colony, $N_0$, is indicated in the plots.

Otherwise, for QRCs growing in $0 \leqslant c_{EGF} < 0.08$ ng ml$^{-1}$ and $c_{EGF} \geqslant 10$ ng ml$^{-1}$, a single exponential growth was found when the cell density at colony border regions increased monotonously with time. However, the greater $c_{EGF}$ the smaller the cell density at the colony border regions. For colonies exhibiting a time-dependent cell density gradient, their kinetic data fitted the exponential law. Conversely, as has been previously reported [33] for colonies growing at constant $V_F$, the cell density gradient remained unchanged for about 1000 min.

It is worth noting that density profiles can only be evaluated from those colonies in which the cell number counting is reliable. Unfortunately, for colonies with the largest $N_0$, and $t \gg t_0$, the appearance of 3D cell domains in the colony bulk and enlarged cells at the colony border turned individual cell counting and cell density determination rather uncertain.

### 3.2. Quasi-linear colonies

QLCs exhibit large cell populations and constant front length that imply a constant free space contribution assisting colony propagation. These runs allowed us to determine cell motility parameters by both manual cell tracking and particle image velocimetry (PIV) [42, 46]. These data help to understand further details of the influence of the spatiotemporal colony heterogeneities on both the local cell morphology and the colony front spreading dynamics.

#### 3.2.1. *Morphology*

The influence of $c_{EGF}$ on the collective phenomena involved in the morphology evolution of QLCs is depicted in figure 6. The effect of $c_{EGF}$ on cell morphology at QLC outer regions is to some extent comparable to that described for confluent small QRCs.

In the absence of EGF, colony pattern microimages taken 24 h after the Teflon removal revealed a gradual local cell density decrease in going from the innermost colony regions outwards. Many cells exhibited an extended cytoplasm polarized in the colony front propagation direction. Also, groups of cells at the bulk oriented towards the colony front can be observed. This morphological feature, which is also applicable at longer $t$ (60 h), is also accompanied by a further cell density increase at inner colony regions, yielding the incipient formation of 3D clusters there and a further increase in the average cell size at the colony border. Likewise, it appears that the presence of oriented cell

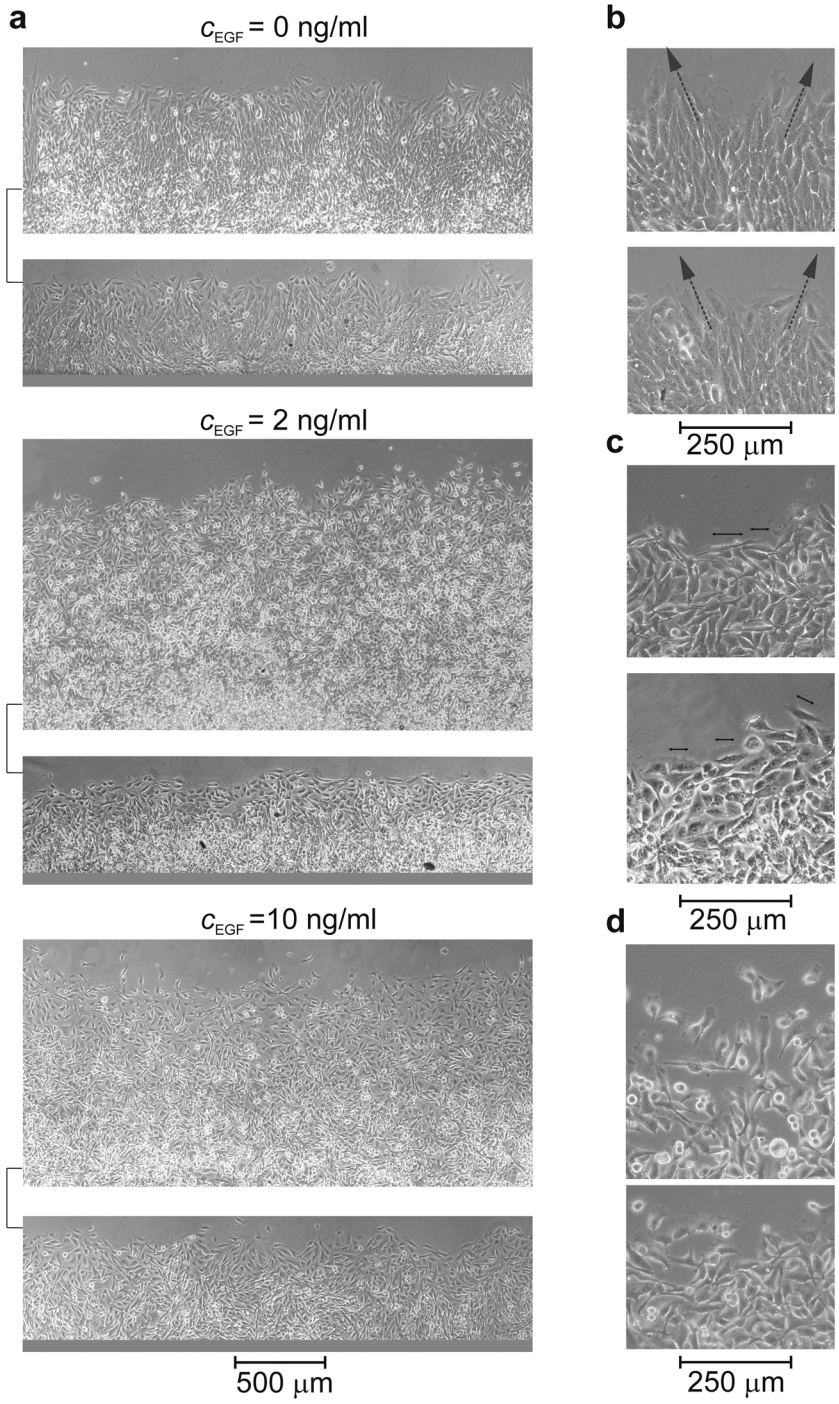


**Figure 6.** QLC patterns. (a) Sequences for cell cultures in media with different $c_{EGF}$ as indicated in the figure. Images were taken at $t = 24$ and $t = 60$ h after the Teflon removal. (b) Enlarged images of cells protruding the contour of a colony growing in the culture medium with $c_{EGF} = 0$; the time between images is 8 h. (c) Images of a colony border sector in the culture medium with $c_{EGF} = 2$ ng ml$^{-1}$; a large number of cells are oriented parallel to the colony border (indicated in the figure by black segments). The time between images is 8 h. (d) Images of a sector of the colony border region. The colony grows in the culture medium with $c_{EGF} = 10$ ng ml$^{-1}$; the detachment of both isolated cells and groups of cells from the colony can be appreciated.

domains is associated with the formation of protrusions at the colony front (figures 6(a) and (b)).

Sequences of colony patterns propagating in EGF-containing media, either with $c_{EGF} = 2$ or 10 ng ml$^{-1}$ at $t = 24$ h and $t = 60$ h, are also depicted in figure 6. For $t = 24$ h, the colony bulk regions exhibit a higher cell density than at the colony border, as in the case of cultures in the control medium. In contrast, in the presence of EGF, the cell average size and the extent and number of colony domains with polarized cells are significantly smaller than in the control medium. As shown in figure 6(c), a large number of cells are oriented parallel to the colony front, whereas other ones in the colony bulk exhibit long filopodia connecting distant neighbor cells. These distinct behaviors are even more remarkable for $t = 60$ h. Otherwise, growth patterns at longer $t$ also involve a large number of rounded cells, either under duplication or partially

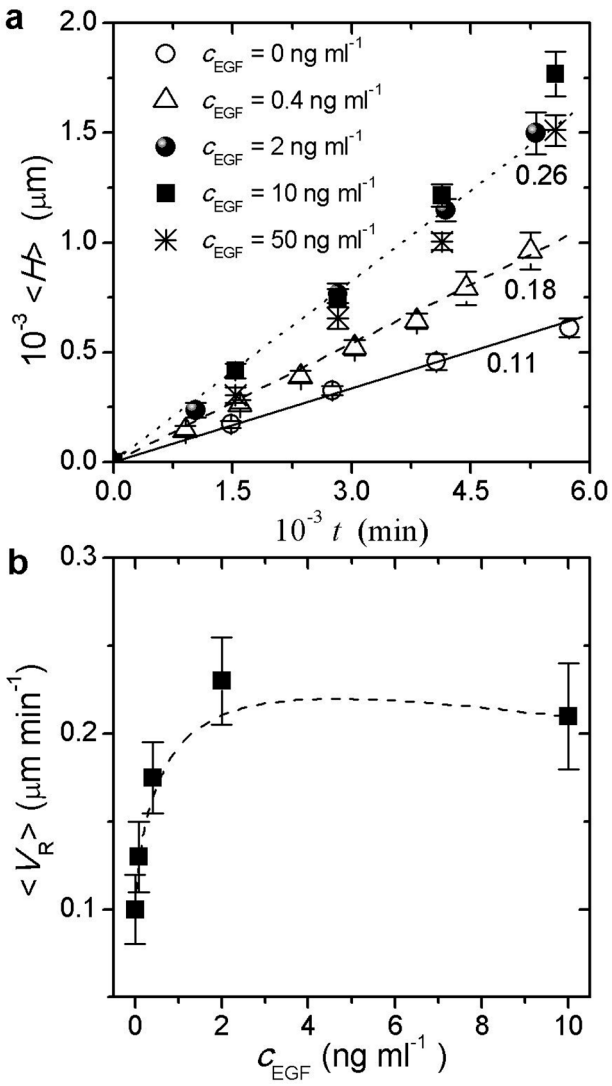


**Figure 7.** (a) Average QLC front displacement distances versus $t$ plots. Data from colonies in culture media containing different $c_{EGF}$. The slopes ($\mu$m min$^{-1}$) of the plotted lines are included. (b) Average colony front displacement velocity of QRC colonies for different $c_{EGF}$ as indicated. Standard errors are included.

detached forming small cell agglomerates. It appears that the presence of EGF induces the enlargement of the 2D low density region particularly near the colony border. But, for $c_{EGF} = 10$ ng ml$^{-1}$ most cells are interconnected through long filopodia. Besides, either individual cells or small groups of cells tend to detach from the colony, generating a less confluent colony border (figures 6(a) and (d)).

### 3.2.2. *Colony propagation kinetics*

The average QLC front displacement operates at constant $V_F$ regardless of $c_{EGF}$, although its magnitude increases from $\langle V_F \rangle = 0.11$ $\mu$m min$^{-1}$ at $c_{EGF} = 0$ ng ml$^{-1}$ and $c_{EGF} = 0.08$ ng ml$^{-1}$ to $\langle V_F \rangle = 0.18$ $\mu$m min$^{-1}$ at $c_{EGF} = 0.4$ ng ml$^{-1}$, and to $\langle V_F \rangle \sim 0.26$ $\mu$m min$^{-1}$ at $c_{EGF}$ 2, 10 or 50 ng ml$^{-1}$ (figure 7(a)). At the highest $c_{EGF}$, the colony front became rougher and exhibited a large number of disaggregated cells, making it rather uncertain for tracing the colony front contour.

The limiting average colony front displacement velocity of QRC colonies $\langle V_R \rangle$, obtained from the slope of $\langle R \rangle$ versus $t$ plots at the linear constant velocity regime, is plotted in figure 7(b). Despite the large error, mainly due to the poor definition of the constant velocity regime, a first rather abrupt increase in $\langle V_R \rangle$ with $c_{EGF}$ and a tendency to attain saturation for $c_{EGF} > 2$ ng ml$^{-1}$ is observed. Moreover, for each $c_{EGF}$, $\langle V_R \rangle$ values are similar to the QLC front displacement velocity, as it has been previously reported for $c_{EGF} = 0$ ng ml$^{-1}$ [33].

### 3.2.3. *Cell motility*

Individual cell trajectories were tracked from QLCs in the control and EGF-containing culture media. The tracking was done considering those cells located at the first three cell layers from the colony border.

For $c_{EGF} = 0$, cell trajectory tracking diagrams at inner colony regions exhibited random cell displacements, whereas at outer colony regions, cell displacements involved a greater directionality. As reported above, QLCs displayed distinguishable distributions of cell density domains and the formation of protru-

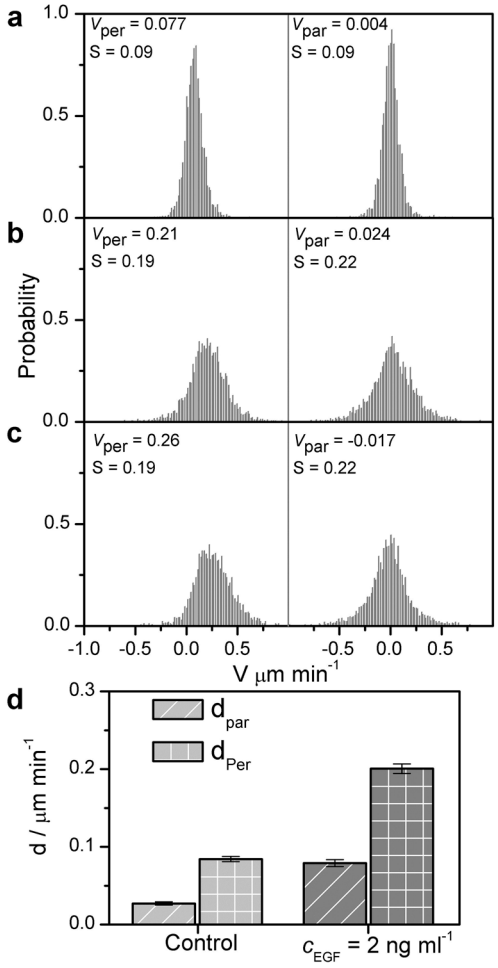


**Figure 8.** (a)–(c) Cell velocity components in control and EGF-containing media from cell trajectory tracking of cells located at the first three cell layers from the colony border: (a) $c_{EGF} = 0$; (b) $c_{EGF} = 2$ ng, cell density = 0.0012 cell $\mu m^{-2}$; (c) $c_{EGF} = 2$ ng, cell density = 0.000 67 cell $\mu m^{-2}$. The mean values and standard deviations (S) are included. (d) Average net parallel, $d_{par}$, and perpendicular, $d_{per}$, displacements every $\Delta t' = 30$ min. Three experiments for each condition and more than 200 cells were considered. Standard errors are included.

sions at the colony border. The cell motility position-dependent characteristics should result from the cell displacement asymmetries in the colony, mainly driven by colony cell density heterogeneities (figure 6). The increase in cell density at the colony inner regions in comparison with border regions enhances cell motility asymmetry, and cell density distribution at different regions of the colony locally affects cell displacements.

The cell trajectory tracking of colonies with $c_{EGF} = 2$ ng ml$^{-1}$ and distinct initial cell densities at the border region, i.e. values close to 0.0012 and 0.00067 cell $\mu m^{-2}$, was analyzed and compared with individual cell trajectories in the control medium. Histograms of cell velocity components parallel $V_{par}$ and perpendicular $V_{per}$ to the colony front are depicted in figures 8(a)–(c). For colonies with initial cell densities close to 0.0012 cells $\mu m^{-2}$, the value of $\langle V_{per} \rangle$ increased from 0.077 $\mu$m min$^{-1}$ in the control medium to 0.21 $\mu$m min$^{-1}$ in $c_{EGF} = 2$ ng ml$^{-1}$ containing medium. Moreover, for a cell density of 0.000 67 cells $\mu m^{-2}$ and $c_{EGF} = 2$ ng ml$^{-1}$, $\langle V_{per} \rangle$ further increased to 0.26 $\mu$m min$^{-1}$. On the other hand, irrespective of the experimental conditions, the value of $\langle V_{par} \rangle$ was close to zero. The standard deviation (S) of both $V_{per}$ and $V_{par}$ increased about twice in the presence of EGF as compared to the control medium.

The presence of EGF also changed the average net parallel ($d_{par}$) and perpendicular ($d_{per}$) displacements of individual cells every 30 min (figure 8(d)). For $c_{EGF} = 2$ ng ml$^{-1}$ and initial average cell density of 0.0012 cell $\mu m^{-2}$, $d_{par} = (2.37 \pm 0.12)$ $\mu$m and $d_{per} = (6.03 \pm 0.18)$ $\mu$m. These figures are larger than those obtained from cells in colonies growing in the control medium, i.e. $d_{par} = (0.81 \pm 0.06)$ $\mu$m and $d_{per} = (2.52 \pm 0.09)$ $\mu$m. Moreover, the quotient $d_{par}/d_{per}$ became larger in the presence of EGF than in the control medium, being $0.39 \pm 0.03$ and $0.31 \pm 0.02$, respectively. Furthermore, the average height of protrusions was smaller in the presence of EGF in comparison to that in the absence of EGF, thus the contribution of parallel displacements should be larger in the former case.

Average log msd versus log $\Delta t$ plots obtained from cell trajectories in colonies propagating in both the control and $c_{EGF} = 2$ ng ml$^{-1}$ containing media exhibited a linear relationship, irrespective of the culture media and cell density at the colony border (figure 9(a)). The slopes of these plots resulted in $1.74 \pm 0.04$ and $1.81 \pm 0.01$ for the control and the EGF-containing medium, respectively. These figures show a small difference in cell motility at the colony border region with a cell density of 0.0012 and 0.000 67 cell $\mu m^{-2}$. Thus, in EGF-containing medium the msd value is higher than in the control medium, a fact that is consistent with a greater average cell velocity at the colony border. Accordingly, for $\Delta t = 30$ min, the average cell velocity is close to 0.3 $\mu$m min$^{-1}$.

The probability of a 45° change in the cell displacement direction is plotted versus the time step (figure 9(b)). In colonies growing in 2 ng ml$^{-1}$ EGF-containing medium, and with cell densities of 0.0012 and 0.000 67 cell $\mu m^{-2}$, the 30 min cell persistence has a probability of 0.45 and 0.35, respectively. In contrast, for cells in the control medium, the same persistence exhibits a probability close to 0.63. This probability, however, decreases faster in the control medium than in the EGF-containing one. In the former case, the above probability approached zero at about 210 min, whereas at the low cell density colony with EGF-containing medium it remained close to 0.05. Therefore, the largest persistence resulted from low cell density colonies growing in the presence of EGF. The persistence versus the average cell displacement distance plot (figure 9(c)) revealed that in EGF-containing medium, both the cell displacement distance and the persistence become greater than in the control medium. Conse-

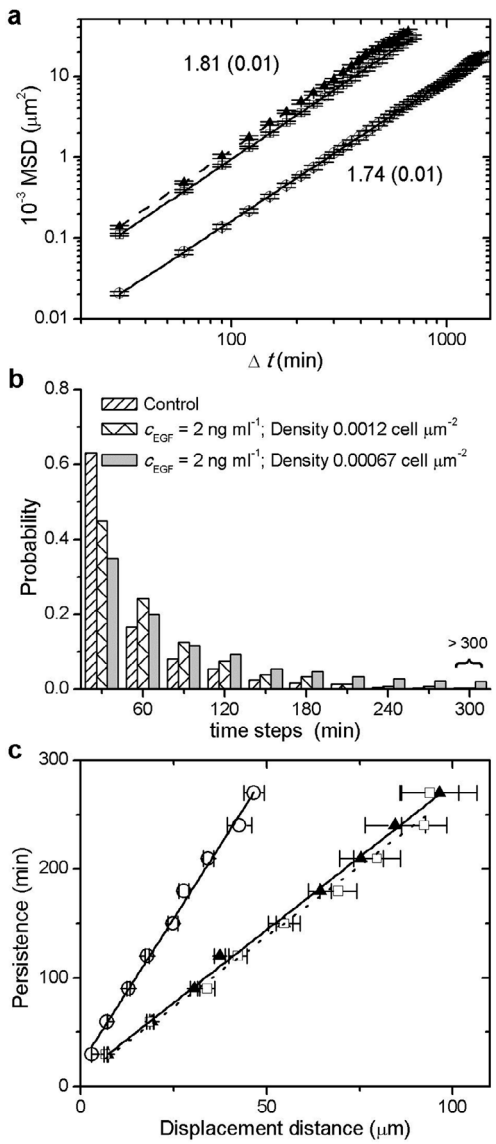


**Figure 9.** (a) Log–log plots of msd versus $\Delta t$ from trajectories of cells in control (○) and 2 ng ml$^{-1}$ EGF-containing media at cell densities of 0.0012 (□) and 0.00067 cell $\mu m^{-2}$ (▲). (b) Probability versus persistence plots from cell trajectories under conditions depicted in (a); the probability of observing persistent movements longer than 300 min is also included. (c) Persistence versus cell displacement distance from the same cell trajectories as in (a).

quently, those cells that move longer distances for a certain time are also the more persistent ones.

PIV data also indicate that cell velocity as well as the extension of the outer colony rim with highly motile cells increased in the presence of EGF (figure 10) as indicated by the color scale. The velocity components show longer vectors in 2 ng ml$^{-1}$ EGF culture medium than for $c_{EGF} = 0$. These data are consistent with the greater extension of the effective colony rim in the presence of EGF, used in the kinetic equation proposed [44]. The analysis of the field velocity components indicates that for $c_{EGF} = 2$ ng ml$^{-1}$, it appears that the increase in the magnitude of the parallel component is larger than that observed for the perpendicular component (figure 10). This fact is in agreement with individual cell trajectory data (figure 8(d)). Furthermore, a trend to a faster increase of the parallel component than the perpendicular component in going from the bulk to the colony border is observed from colonies growing in EGF-containing medium (figure 10(b)).

### 3.2.4. *Roughness fluctuation*

According to the dynamic scaling theory [26], the interfacial roughness of a growing front of size $L$, $w(L, t)$, is expected to increase for $t \ll t_s$, where $t_s$ is the roughness saturation time

$$w \propto t^{\beta} \quad t \ll t_s \tag{5}$$

and when $t > t_s$, roughness saturation $w_s$ is attained. Then, $w_s$ should increase with $L$ according to

$$w_s \propto L^{\alpha} \quad t \gg t_s. \tag{6}$$

Moreover, the value of $t_s$ depends on the system size

$$t_s \propto L^{Z} \quad z = \alpha/\beta \tag{7}$$

$z = \alpha/\beta$ being the dynamic exponent.

Accordingly, for a set of scaling exponents one expects the fulfillment of the Family–Vicsek relation

$$\frac{w(L,t)}{L^{\alpha}} \propto f\left(\frac{t}{L^{Z}}\right). \tag{8}$$

On the other hand, a more generic scaling analysis considers the structure factor $S(k,t)$ of the entire ($s = L$) growth front [26, 47, 48]

$$S(k,t) = k^{-(2\alpha_s+1)} f\left(kt^{1/Z}\right) \tag{9}$$

where $\alpha_s$ is the spectral roughness exponent and $f$ ($x = kt^{1/z}$) the scaling function that depends on $x$ as follows

$$f(x) = \begin{cases} \text{const} & \text{for } x \gg 1 \\ x^{(2\alpha_s+1)} & \text{for } x \ll 1 \end{cases}. \tag{10}$$

The advantage of estimating the scaling exponents in the Fourier space instead of in the real space is that in the former case only long wavelength modes contribute to the front scaling. Real space scaling (equation (8)) involves all wavelength modes, including short ones, so that stronger finite size effects should be expected.

In the presence of EGF, within a range of $t$ and $l$ that differs from that of colonies growing in the control medium [30], the KPZ equation provides a reasonable description of the colony front dynamics (figure 11). Hence, values of $\alpha$ from $w$ versus $L$, as well as $\alpha_s$ from the Fourier analysis, confirm that colony front roughness fluctuations fulfill, at least for certain range of $l$ and $t$, the standard KPZ equation (figure 11).

Otherwise, $w(l, t)$ versus $t$ plots from different front sizes, $l$, are depicted in figure 12. In the control medium, the colony front exhibits roughness saturation in the range $200 \leqslant l \leqslant 1200$ $\mu$m; for $l > 1200$ $\mu$m a linear log–log relationship with a slope $\beta$ close to 0.34 results, as predicted by the KPZ equation. The presence

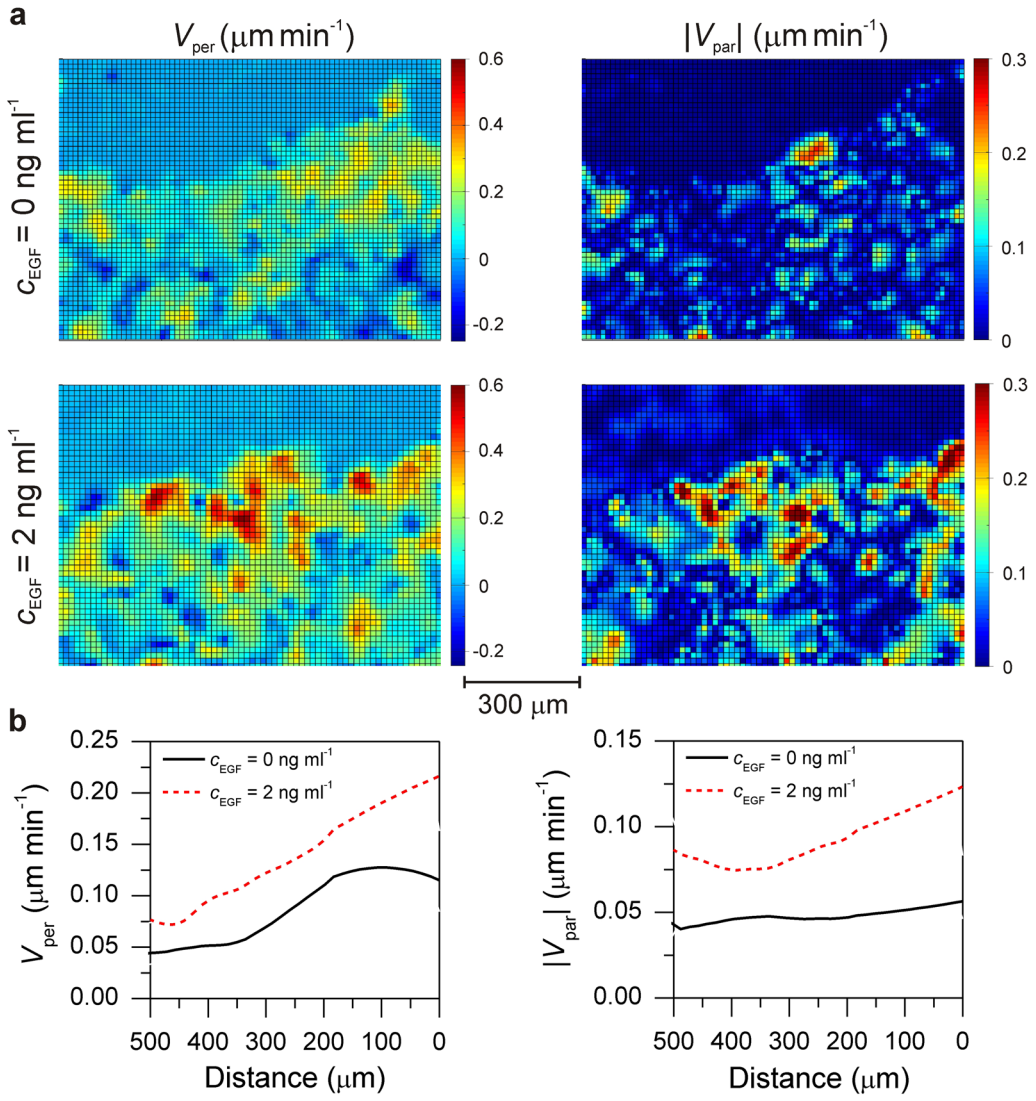


**Figure 10.** (a) Velocity field images for HeLa QLCs growing in the control medium and 2 ng ml$^{-1}$ EGF-containing medium as indicated. The values of $V_{per}$ and $|V_{par}|$ are indicated in color scale. (b) Average $V_{per}$ and $|V_{par}|$ versus distance to the colony border plots, calculated from (a).

of EGF in the medium increases the roughness of the colony front, at both the colony and the cellular scales. Data from colonies propagating in $c_{EGF} = 2$ ng ml$^{-1}$ culture medium indicate that the front roughness increases continuously without saturation for $l$ up to 900 $\mu$m, but saturation occurs at larger $l$ values. Surprisingly, for $c_{EGF} = 10$ ng ml$^{-1}$ in the culture medium, the roughness saturation is better observed only at intermediate values of $l$.

## 4. Discussion

### 4.1. Kinetics and cell morphology aspects of QRCs and QLCs in EGF-containing medium

HeLa cells are sensitive to the presence of EGF, since after binding with a cell surface receptor it activates different signaling pathways [49]. Therefore, both individual cell and the whole colony morphology depend on $c_{EGF}$ (figures 1 and 2). The presence of EGF decreased the size of focal contacts, although their number per cell increased, attaining a saturation effect as concluded from figure 2. This is a relevant fact that agrees with fast kinetics for the adhesion/detachment process [50, 51]. Likewise, those changes in cytoskeletal organization and focal contact characteristics correlate with cell motility behavior [36].

Data have shown that QRCs exhibit a $c_{EGF}$ dependent morphology evolution and propagation kinetics (figures 3 and 4). The effect of $c_{EGF}$ on these processes depends mainly on $N_0$ and the local cell density. In general, for relatively large $N_0$ and colony cell densities, a linear increase in the average colony radius prevails, whereas for both relatively small $N_0$ and colony cell densities, the supra-exponential behavior at the initial kinetic stages of growth, followed by the exponential regime, is observed. Cell density evolution and the $N$ versus $t$ exponential relationship for $0.4 \leqslant c_{EGF} \leqslant 2$ ng ml$^{-1}$(figure 7), indicate that the supra-exponential growth could be mainly due to the contribution of cell size and cell–cell distance increase, change in shape

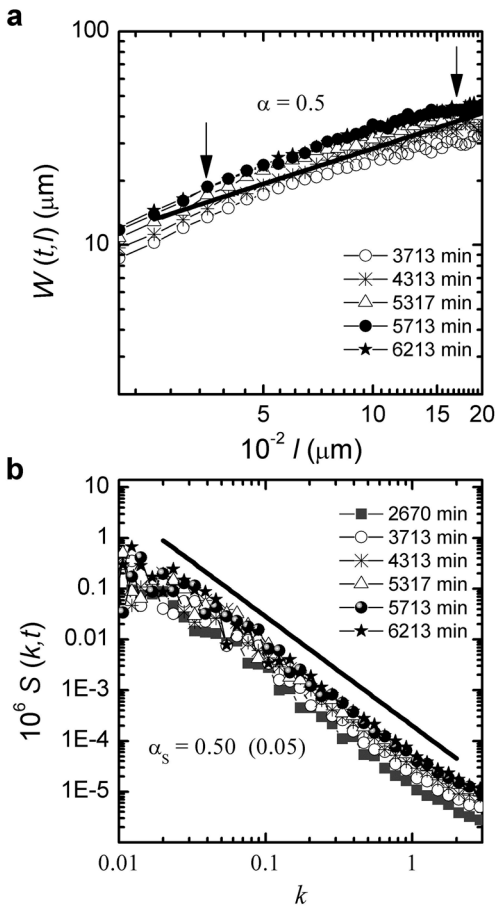


**Figure 11.** $W(l, t)$ versus $\log l$ (a) and $S(k, t)$ versus $k$ (b) log–log plots from colonies with $c_{EGF} = 2\,\text{ng ml}^{-1}$.

and the enhanced cell motility at the monolayer (figures 8–10), and consequently a more effective colony contour propagation (figures 3 and 4).

Proposed colony growth models [28, 44, 45] have considered that the radial cell colony propagation comprises three stages, namely, a diffusion regime that follows a $\langle R\rangle$ versus $t^{1/2}$ relationship, followed by an exponential regime, and a subsequent decrease in the colony propagation velocity characterized by a linear relationship between $\langle R\rangle$ and $t$ [44]. It should be noted that in experiments with confluent colonies growing in standard culture medium, the first kinetic regime disappeared and only the exponential growth regime followed by the constant velocity regime set in [28, 45].

This behavior has been mathematically described by a two-part equation [44] where the growing colony cross-section was approached as an outer ring of effective thickness $\Delta L_{\text{eff}} = R(t) - R_2(t)$ and a central core of instantaneous radius $R_2(t)$ associated with the delaying effect. Then, at $t = 0$, $N = N_0$, and $R = R_0 < \Delta L_{\text{eff}}$, the transition from the exponential to constant velocity regime has been successfully obtained, in agreement with experimental data [33].

The colony dynamics involves a number of processes that influence the global behavior of the system. Each process contribution depends on the growing stage of the colony, and on the growing conditions, namely $c_{EGF}$, the colony population, the colony age, among others, and cooperates to render the global properties of the system. The proposed equation [44] is an interesting contribution that reflects the global heterogeneities developed during the colony growth. The model simplifies the description employing macroscopic variables rather than the follow-up of the evolution of each component and the medium interacting with them.

In this case, based upon the preceding results, within a certain $c_{EGF}$ range, the fast increase in the colony radius at the first stages of growth is enhanced. Then, the $t^{1/2}$ term become relevant and can be introduced in the equation proposed in [44], taking into account the different initial conditions ($N_0$, colony cell density, and $c_{EGF}$). Then, the modified equation resulted in

$$\langle R\rangle = \begin{cases} A\,(\tau^{-1}+\phi)\,t^{1/2} + A'\exp\left(\frac{t}{2\tau}\right) & t \leqslant t_c \\ \pi^{1/2}\frac{\Delta L_{\text{eff}}}{2}\left[1 + W\left(\frac{A'^2 r_c^2}{\pi \Delta L_{\text{eff}}^4}\right)\exp\left(1+\frac{2t}{\tau}\right)\right] & t > t_c \end{cases} \quad (11)$$

with $W(x)$ being the Lambert function, $(r_c)$ the cell radius, $(\tau)$ its duplication time, $(A')$ the initial colony radius, $B = A(\tau^{-1} + \phi)$ a fitting the parameter with $A$, a constant associated with the initial colony characteristics and $\phi$ the cell diffusivity, and $t_c$ the transition time to the constant colony front velocity regime. The latter is approached as $\Delta L_{\text{eff}}$ attains a constant value. The plot of our experimental data according to equation (11), considering the colony growth conditions, listed in table 1, resulted in a reasonable agreement (figure 4).

The departure from the exponential growth regime at the first stages of growth should be favored in QRCs with small $N_0$, but with an appropriate cell density value where the contribution of cell diffusion could be distinguished. Similarly, for sufficiently large values of $N_0$, the higher $c_{EGF}$ the larger $\Delta L_{\text{eff}}$, and consequently, the longer $t_c$.

The values of $\langle V_R\rangle$ from QRCs growing at the constant velocity regime for each $c_{EGF}$ approach those obtained from QLCs with the same $c_{EGF}$. QLCs involve large $N_0$ and high density domains at inner regions, and exhibit a constant velocity growth regime, attaining a limiting value $\langle V_F\rangle = 0.26 \pm 0.05\,\mu\text{m min}^{-1}$ irrespective of $c_{EGF}$, from $c_{EGF} > 2\,\text{ng ml}^{-1}$ (figure 7). This $\langle V_F\rangle$ value was three times larger than in the control medium. For QLCs, the $\Delta L_{\text{eff}}$ is formed almost immediately, and no transient can be distinguished.

For $c_{EGF} \geqslant 10\,\text{ng ml}^{-1}$, the detachment of both individual cells and groups of cells from the colony (figure 6), which could be related to the loose cell–cell adhesions in the colony, is observed. Cell shape and size, and their orientation in relation to the colony contour, change dramatically in the presence of EGF. In the next section, cell motility characteristics are discussed in order to explain the contribution of the above morphological changes.

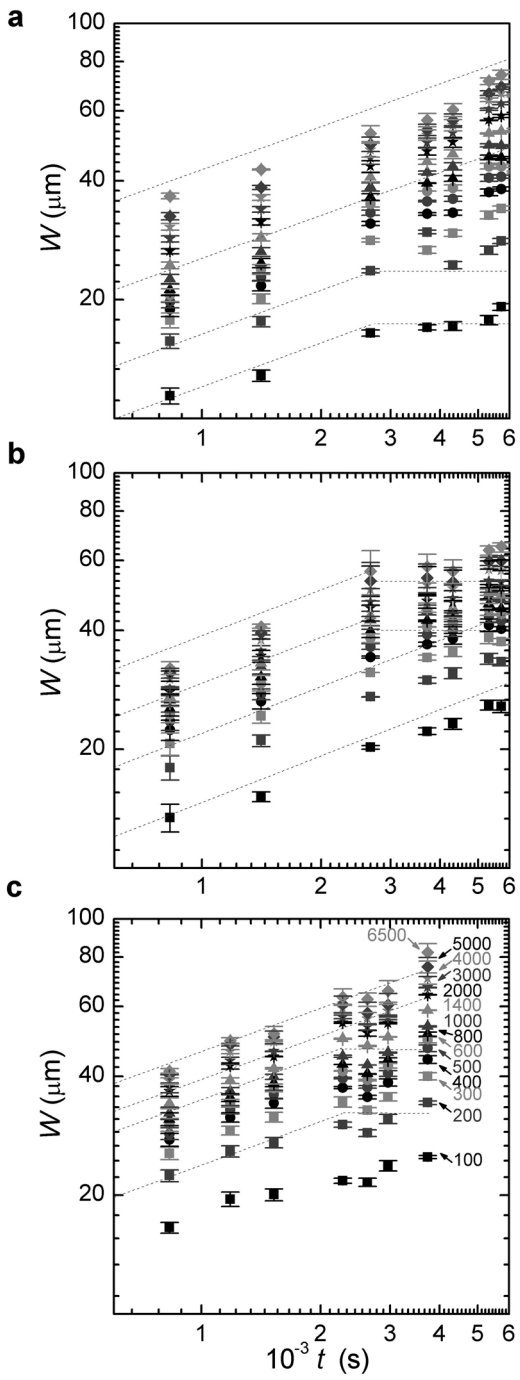


**Figure 12.** $W(l, t)$ versus $t$ log–log plots for different $l$. Binned data from five QLCs propagating in different media. (a) Control medium, (b) with $c_{EGF} = 2\,ng\,ml^{-1}$, and (c) with $c_{EGF} = 10\,ng\,ml^{-1}$. Roughness was analyzed for values of $l$ indicated in (c). Standard error bars are indicated.

### 4.2. Individual cell motility behavior from QLCs

Correlations between cell motility characteristics and the global dynamics of the QRCs and QLCs were also approached considering that cell displacements can be tackled roughly by transport equations either disregarding or taking the cell size as variable [52, 53]. Thus, it is possible to map transport equations that involve no linear diffusion contributions to general complex condensed phase growth equations [26] such as those proposed from the dynamic scaling analysis. Likewise, the processes described for QRC take place at a size scale that would affect the QLC dynamics locally. The increase in the collective behavior of HeLa cell displacement with the size of QRCs should be mainly attributed to a crowding effect [33]. The latter is enhanced in QLCs due to space restrictions [54], which only exhibit a constant $V_F$ regime. For QRCs with large $N_0 > 1200$ and cell density larger than 0.0026 cell $\mu m^2$, the colony propagates at constant velocity. The supra-exponential coupling to the exponential regime would be observed in colonies with a cell number and density appropriate to generate a cooperative effect on the colony propagation based on changes in cell shape and separation, duplication, and migration.

Our results show that in the presence of EGF, cell displacements are more persistent and ballistic (figure 9), as reported, for instance, for mammary epithelial cell migration [55]. Furthermore, in our case, an increase in the cell average lateral displacement with respect to the forward one (figures 8(d) and (10)) was observed. The colony density influences the cell velocity magnitude, the larger the latter the lower the cell density (figures 8 and 9). Moreover, for intermediate values of $c_{EGF}$ ($0.08 \leqslant c_{EGF} \leqslant 2\,ng\,ml^{-1}$) cells appear to be connected by long filopodia and at the border region, they tend to form small groups of moving cells.

PIV data (figure 10) indicate that in the presence of EGF the cell velocity is larger than that resulting from colonies growing in the control medium, and maintains a value larger than a half of the maximum cell velocity for distances from the colony border twice the one measured for the control medium. Correspondingly, the effective rim significantly increases in the presence of EGF, in agreement with the preceding kinetic data that indicate that the extension of the outer colony rim with highly motile cells increases in the presence of EGF, and the velocity components show longer vectors in 2 - 10 ng $ml^{-1}$ EGF culture medium than for $c_{EGF} = 0$. Moreover, PIV data show a larger contribution of lateral displacements in the presence of EGF, in consonance with individual cell trajectories, cell morphology and its relative orientation respect to the colony border (figure 6).

Colony propagation data plotted as $\langle R \rangle$ and $\langle H \rangle$ versus $t$ (figure 7) exhibit a tendency to attain a limiting value for the colony propagation velocity as $c_{EGF}$ increases. This fact indicates that the EGF-enhanced cell motility would also reach saturation. A similar behavior has been reported for MCF-7 breast cancer cells stimulated with IGF (insulin growth factor) in a migration assay [56]. In our experiments, it should be pointed out that for the largest $c_{EGF}$ the detachment of individual cells and groups of cells would make the analysis rather unfeasible. For colonies remaining confluent, the increase in $c_{EGF}$ in the range $0.08 < c_{EGF} < 2$–$10\,ng\ ml^{-1}$produces an increase in cell duplication, as well as changes in cell morphology and in the number and size of focal contacts. In

**Table 1.** QLC growth conditions, $c_{EGF}$; cell colony initial properties, $N_0$ and $A'$; cell duplication time, $\tau$; cell average radius, $r_c$; fitting parameters $B$ and $\Delta L_{eff}$ employed to describe experimental data with equation (11).

| Colony growth conditions | | | | | | Fitting parameters | |
|---|---|---|---|---|---|---|---|
| $c_{EGF}$/ng ml$^{-1}$ | $N_0$ | $r_c/\mu$m | Cell density/$N$ $\mu$m$^{-2}$ | $\tau$/min | $A'/\mu$m | $B$ $\mu$m min$^{-1/2}$ | $\Delta L_{eff}/\mu$m |
| 0 | 16 | 16 | 0.001 24 | 3250 | 64 | 0 | 200 |
| 0.4 | 430 | 20.8 | 0.000 74 | 3200 | 360 | 0.0792 | 240 |
| 10 | 1338 | 10.8 | 0.002 72 | 2800 | 317 | 0.10144 | 440 |

any case, all these changes are coupled and depend on time, i.e., the colony age, location in the colony and the developed heterogeneities.

### 4.3. Dynamic scaling analysis

Results from the dynamic scaling analysis of both QRC and QLC fronts in the control medium for either transformed or tumor cells revealed that, at least for certain ranges of $t$ and $l$, their dynamics fulfill the Kardar–Parisi–Zhang equation [30, 57]. The scaling analysis of colony contour roughness fluctuations for different $c_{EGF}$ allows us to envisage a colony growth dynamics compatible with the standard KPZ equation in ranges of $t$ and $l$ different than in the control medium (figures 11 and 12). At constant $l$, a clear roughness saturation was observed in the presence of EGF, particularly for $c_{EGF} = 2$ ng ml$^{-1}$ (figure 12). It is worth noting that for QLCs in media with EGF, and for $l < 300$ $\mu$m, contrarily to the expected behavior, roughness saturation was absent. At this length scale, the changes in cell size and morphology and the rapid membrane fluctuations produced by the EGF would interfere with the colony contour scaling properties.

These results can be associated with previously described colony characteristics. Thus, in growth media with EGF, cells become more tapered and acquire an orientation parallel to the colony front. The persistence and the ballistic characteristics of cell displacements are enhanced in polarized, fast moving cells that appear in this culture medium. Concomitantly, the colony front displacement velocity reaches a maximum value within the range $2 \leqslant c_{EGF} < 10$ ng ml$^{-1}$, and the colony border remains confluent along the follow-up for $c_{EGF}$ up to 10 ng ml$^{-1}$, with a larger contribution of cell displacement parallel to the colony front in comparison with data from colonies in the absence of EGF, promoting the earliest saturation of the roughness contour in the presence of EGF. This fact can be interpreted by the relevance of the nonlinear term in the standard KPZ equation related to the lateral growth and parallel correlation length.

For $c_{EGF} \geqslant 10$ ng ml$^{-1}$, a fraction of either individual cells or groups of them are likely to detach from the colony. As shown in figure 12(c), this process increases the roughness of the colony contour, and the roughness saturation is roughly observed; furthermore, for this condition the contour definition begins to fail, as has been commented for QRC and small $N_0$. These distinct EGF-induced cell behaviors observed for intermediate values of $c_{EGF}$ are also consistent with the observation of cell motility reported in the literature [36, 58]. Furthermore, the results corroborate the usefulness of the proposed growth equation and settle a bridge between processes at the cellular and colony scale.

## 5. Conclusions

- The epidermal growth factor (EGF) affects cell–cell interactions and promotes a fast cell displacement, leading to sparse cell colonies. In the presence of EGF, to attain confluent colonies, large values of $N_0$ and initial cell densities are required.
- Data comparison of colonies growing in control medium with those in EGF—containing medium indicates that EGF produces morphological changes at the cell and colony levels. The presence of EGF enhances the appearance of cells with large filopodia, cell orientation in the direction parallel to the growth front, and eventually cell detachment from the colony, rendering a colony border region with a lower cell density that extends longer distances from the colony border inwards.
- Colonies growing in EGF-containing medium exhibit average radius versus $t$ plots with a transition from exponential kinetics to a constant $V_F$, as in the case of colonies growing in the control medium. Furthermore, mitogenic and chemotactic properties of EGF perturbed the QRC border displacement kinetics, by increasing the front displacement velocity and the magnitude of both $t_c$ and $R_c$, and producing a supra-exponential growth regime at earlier stages of growth for colonies with intermediate values of $N_0$ and cell densities.
- The presence of EGF increases the individual cell velocity and affects the contribution of velocity components parallel to the colony front, as well as the persistence and ballistic characteristics of cell trajectories. Moreover, as $c_{EGF}$ is increased, cells from deeper layers of the colony have net velocities towards the colony front and also contribute to the propagation of the colony.
- The growth kinetics of colonies in EGF-containing medium is reasonably adjusted by a mathematical model proposed in [44] including a $t^{1/2}$ term to fit the supra-exponential growth

at the earlier stages of growth. Then, this model agrees with the increase in the effective rim and $t_c$ caused by the presence of EGF in the medium.

* In comparison with colonies growing in the control medium without EGF, at intermediate values of $c_{EGF}$, persistent cooperative cell displacements in the border regions influence the roughening of the colony contour, which is reasonably described by the standard Kardar-Parisi-Zhang growth model with faster roughness saturation.

The presented strategy is suitable to study the effects of other growth factors that modify the cellular phenotype and affect the colony evolution. The results of this work are of general interest for the development of feasible models to describe complex systems as well as to improve strategies and protocols in the field of wound healing and cancer research.

## Acknowledgments

This work was supported by the Consejo Nacional de Investigaciones Científicas y Técnicas of Argentina, CONICET (PIP 0602), the Comisión de Investigaciones Científicas (CIC), Pcia. Bs. As., Agencia Nacional de Promoción Científica y Tecnológica (ANPCyT, Argentina; PICT-163/08, PICT-2010-2554, and PICT-2013-0905), the Austrian Institute of Technology GmbH (AIT–CONICET Partner Group: 'Exploratory Research for Advanced Technologies in Supramolecular Materials Science', Exp. 4947/11, Res. No. 3911, 28-12-2011), and Universidad Nacional de La Plata (UNLP). MAP and OA are staff members of CONICET.

## ORCID iDs

M A Pasquale https://orcid.org/0000-0002-0416-100X

## References

[1] Wells A 2006 *Cell Motility in Cancer Invasion and Metastasis* (The Netherland: Springer)
[2] Simpson C L, Patel D M and Green K J 2011 Deconstructing the skin: cytoarchitectural determinants of epidermal morphogenesis *Nat. Rev. Mol. Cell Biol.* **12** 565
[3] Behm B, Babilas P, Landthaler M and Schreml S 2012 *Cytokines, chemokines and growth factors in wound healing J. Eur. Acad. Dermato. Venereol.* **26** 812
[4] Borena B M, Martens A, Broeckx S Y, Meyer E, Chiers K, Duchateau L and Spaas J H 2015 Regenerative skin wound healing in mammals: state-of-the-art on growth factor and stem cell based treatments *Cell Physiol. Biochem.* **36** 1
[5] Ceresa B P and Peterson J L 2014 International review of cell and molecular biology *Cell and Molecular Biology of Epidermal Growth Factor Receptor* vol 313, ed J Kwang (Waltham: Elsevier) ch 5, p 145
[6] Mitsudomi T and Yatabe Y 2010 Epidermal growth factor receptor in relation to tumor development: EGFR gene and cancer *FEBS J.* **277** 301
[7] Maheshwari G, Wells A, Griffith L G and Lauffenburger D A 1999 Biophysical integration of effects of epidermal growth factor and fibronectin on fibroblast migration *Biophys. J.* **76** 2814
[8] Kurten R C, Chowdhury P, Sander R Jr, Pittman L M, Sessions L W, Chambers T C, Lyle C S, Schnackenberg B J and Jones S M 2005 Coordinating epidermal growth factor-induced motility promotes efficient wound closure *Am. J. Physiol. Cell Physiol.* **288** C109
[9] Berkers J A, van Bergen en Henegouwen P M and Boonstra J 1991 Three classes of epidermal growth factor receptors on HeLa cells *J. Biol. Chem.* **266** 922
[10] Capuani F, Conte A, Argenzio E, Marchetti L, Priami C, Polo S, Di Fiore P P, Sigismund S and Ciliberto A 2015 Quantitative analysis reveals how EGFR activation and downregulation are coupled in normal but not in cancer cells *Nat. Commun.* **6** 7999
[11] Dürer U, Harting R, Bang S, Thim L and Hoffmann W 2007 TFF3 and EGF induce different migration patterns of intestinal epithelial cells *in vitro* and trigger increased internalization of E-cadherin *Cell. Physiol. Biochem.* **20** 329
[12] Seeger M A and Paller A S 2015 The roles of growth factors in keratinocyte migration *Adv. Wound Care* **4** 213
[13] Pope M D, Graham N A, Huang B K and Asthagiri A R 2008 Automated quantitative analysis of epithelial cell scatter *Cell Adh Migr.* **2** 110
[14] Ware M F, Wells A and Lauffenburger D A 1998 Epidermal growth factor alters fibroblast migration speed and directional persistence reciprocally and in a matrix-dependent manner *J. Cell Sci.* **111** 2423
[15] Geum D T, Kim B J, Chang A E, Hall M S and Wu M 2016 Epidermal growth factor promotes a mesenchymal over an amoeboid motility of MDA-MB-231 cells embedded within a 3D collagen matrix *Eur. Phys. J. Plus* **131** 8
[16] Kim C S, Mitchell I P, Dosetell A W, Kreeger P K and Masters K S 2016 Immobilized epidermal growth factor stimulates persistent, directed keratinocyte migration via activation of PLC$\gamma$1 *FASEB J.* **30** 2580–90
[17] Wickert L E, Pomerenke S, Mitchell I, Masters K S and Kreeger P K 2016 Hierarchy of cellular decisions in collective behavior: implications for wound healing *Sci. Rep.* **6** 20139
[18] Friedl P and Glimour D 2009 Collective cell migration in morphogenesis, regeneration and cancer *Nat. Rev. Mol. Cell Biol.* **10** 445
[19] Haeger A, Wolf K, Zegers M M and Friedl P 2015 Collective cell migration: guidance principles and hierarchies *Trends Cell Biol.* **25** 556
[20] Rappel W J 2016 Cell–cell communication during collective migration *Proc. Natl Acad. Sci. USA* **113** 1471
[21] Ellison D *et al* 2016 Cell–cell communication enhances the capacity of cell ensembles to sense shallow gradients during morphogenesis *Proc. Natl Acad. Sci. USA* **113** E679–88
[22] Chepizhko O *et al* 2016 Bursts of activity in collective cell migration *Proc. Natl Acad. Sci. USA* **113** 11408
[23] Galeano J, Buceta J, Juarez K, Pumariño B, de la Torre J and Iriondo J M 2003 Dynamical scaling analysis of plant callus growth *Europhys. Lett.* **63** 83
[24] Bonachela J A, Nadell C D, Xavier J B and Levin S A 2011 Universality in bacterial colonies *J. Stat. Phys.* **144** 303
[25] Takeuchi K A 2014 Experimental approaches to universal out-of-equilibrium scaling laws: turbulent liquid crystal and other developments *J. Stat. Mech.* **2014** P01006
[26] Barabasi A L and Stanley H E 1993 *Fractal Concepts in Surface Growth* (Cambridge: Cambridge University Press)
[27] Meakin P 1998 *Fractals, Scaling and growth far from Equilibrium* (Cambridge: Cambridge University Press)
[28] Block M, Schöll E and Drasdo D 2007 Classifying the expansion kinetics and critical surface dynamics of growing cell populations *Phys. Rev. Lett.* **99** 248101
[29] Huergo M A C, Pasquale M A, González P H, Bolzán A E and Arvia A J 2011 Dynamics and morphology characteristics of cell colonies with radially spreading growth fronts *Phys. Rev.* E **84** 021917
[30] Huergo M A C, Pasquale M A, González P H, Bolzán A E and Arvia A J 2012 Growth dynamics of cancer cell colonies and their comparison with noncancerous cells *Phys. Rev.* E **85** 011918
[31] Moon K-W, Kim D-H, Yoo S-C, Cho C-G, Hwang S, Kahng B, Min B-C, Shin K-H and Choe S-B 2013 Distinct universality

classes of domain wall roughness in two-dimensional Pt/Co/Pt films *Phys. Rev.* E **110** 107203
[32] Almeida R A L, Ferreira S O, Oliveira T J and Aarão Reis F D A 2014 Universal fluctuations in the growth of semiconductor thin films *Phys. Rev.* B **89** 045309
[33] Muzzio N E, Pasquale M A, González P H and Arvia A J 2014 Influence of individual cell motility on the 2D front roughness dynamics of tumour cell colonies *J. Biol. Phys.* **40** 285
[34] Chen J, Zeng F, Farrester S J, Eguchi S, Zhang M-Z and Harris R C 2016 Expression and function of epidermal growth factor receptor in physiology and disease *Phys. Rev.* **96** 1025
[35] Treloar K K, Simpson M J, Haridas P, Manton K J, Leavesley D, Elwain D L S M and Baker R E 2013 Multiple types of data are required to identify the mechanisms influencing the spatial expansion of melanoma cell colonies *BMC Syst. Biol.* **7** 137
[36] Hou Y, Heldberg S and Schneider I C 2012 Differences in adhesion and protrusion properties correlate with differences in migration speed under EGF stimulation *BMC Biophys.* **5** 8
[37] Sawyer C, Sturge J, Bennett D C, O'Hare M J, Allen W E, Bain J, Jones G E and Vanhaesebroeck B 2003 Regulation of breast cancer cell chemotaxis by the phosphoinositide 3-kinase p110delta *Cancer Res.* **63** 1667
[38] Poujade M, Grasland-Morgain E, Hertzog A, Chavrier P, Ladoux B, Buguin A and Silberzan P 2007 Collective migration of an epithelial monolayer in response to a model wound *Proc. Natl Acad. Sci. USA* **104** 15988
[39] Horzum U, Ozdil B and Pesen-Okvur D 2014 Step-by-step quantitative analysis of focal adhesions *MethodsX* **1** 56
[40] Diambra L, Cintra L C, Chen Q, Schubert D and da Costa L F 2006 Cell adhesion protein decreases cell motion: statistical characterization of locomotion activity *Physica* A **365** 481–90
[41] Li L, Wang B H, Moalim-Nour S, Mohib K, Lohnes D and Wang L 2010 2010 Individual cell movement, asymmetric colony expansion, rho-associated kinase, and E-cadherin impact the clonogenicity of human embryonic stem cells *Biophys. J.* **98** 2442
[42] Petitjean L, Reffay M, Grasland-Mongrain E, Poujade M, Ladoux B, Buguin A and Silberzan P 2010 Velocity fields in a collectively migrating epithelium *Biophys. J.* **88** 1790
[43] Thielicke W and Stamhuis E 2014 PIVlab - Towards User-friendly, Affordable and Accurate Digital Particle Image Velocimetry in MATLAB *J. Open Res. Softw.* **2** e30
[44] Radszuweit M, Block M, Hengstler J G, Schöll E and Drasdo D 2009 Comparing the growth kinetics of cell populations in two and three dimensions *Phys. Rev.* E **79** 051907
[45] Drasdo D 2005 Coarse graining in simulated cell populations *Adv. Complex Syst.* **8** 319
[46] Muzzio N E, Pasquale M A, Huergo M A C, Bolzán A E, González P H and Arvia A J 2016 Spatio-temporal morphology changes in and quenching effects on the 2D spreading dynamics of cell colonies in both plain and methylcellulose-containing culture media *J. Biol. Phys.* **42** 477
[47] Ramasco J, López J M and Rodríguez M A 2000 Generic dynamic scaling in kinetic roughening *Phys. Rev. Lett.* **84** 2199
[48] López J M, Rodríguez M A and Cuerno R 1997 Superroughening versus intrinsic anomalous scaling of surfaces *Phys. Rev.* E **56** 3993
[49] Oda K, Matsuoka Y, Funahashi A and Kitano H 2005 A comprehensive pathway map of epidermal growth factor receptor signaling *Mol. Syst. Biol.* **1** 1
[50] Xie H, Pallero M A, Gupta K, Chang P J, Ware M F, Witke W, Kwiatkowski D J, Lauffenburger D A, Murphy-Ullrich J E and Wells A 1998 EGF receptor regulation of cell motility: EGF induces disassembly of focal adhesions independently of the motility-associated PLCgamma signaling pathway *Cell Sci.* **111** 615
[51] Rijken P J, Hage W J, Henegouen P M P V E, Verkleij A J and Boonstra J 1991 Epidermal growth factor induces rapid reorganization of the actin microfilament system in human A431 cells *J. Cell Sci.* **100** 491
[52] Deroulers C, Aubert M, Badoual M and Grammaticos B 2009 Modeling tumor cell migration: From microscopic to macroscopic models *Phys. Rev.* E **79** 031917
[53] Simpson M J, Baker R E and McCue S W 2011 Models of collective cell spreading with variable cell aspect ratio: a motivation for degenerate diffusion models *Phys. Rev.* E **83** 021901
[54] Marel A-K, Zorn M, Klingner C, Wedlich-Söldner R, Frey E and Rädler J O 2014 Flow and diffusion in channel-guided cell migration *Biophys. J.* **107** 1054
[55] Maheshwari G, Wiley H S and Lauffenburger D A 2001 Autocrine epidermal growth factor signaling stimulates directionally persistent mammary epithelial cell migration *J. Cell. Biol.* **155** 1123
[56] Simpson M J, Chris Towne, Sean MacElwain D L and Upton Z 2010 Migration of breast cancer cells: Understanding the roles of volume exclusion and cell-to-cell adhesion *Phys. Rev.* E **82** 041901
[57] Kardar M, Parisi G and Zhang Y-C 1986 Dynamic scaling of growing interfaces *Phys. Rev. Lett.* **56** 889
[58] Harms B D, Bassi G M, Horwitz A L and Lauffenburger D A 2005 Directional persistence of EGF-induced cell migration is associated with stabilization of lamellipodial protrusions *Biophys. J.* **88** 1479